NUMERICAL SIMULATION AND ANALYSIS OF HORSESHOE-SHAPED VORTEX IN NEAR-WALL REGION OF TURBULENT BOUNDARY LAYER

Shi Wanli[1], *Ge Ning*[1], *Chen Lin*[2], *Tang Dengbin*[2]

(1. College of Energy and Power Engineering, NUAA, 29 Yudao Street, 210016, Nanjing, P. R. China;
2. College of Aerospace Engineering, NUAA, 29 Yudao Street, 210016, Nanjing, P. R. China)

Abstract: The low-Reynolds-number full developed turbulent flow in channels is simulated using large eddy simulation (LES) method with the preconditioned algorithm and the dynamic subgrid-scale model, with a given disturbance in inlet boundary, after a short development section. The inlet Reynolds number based on momentum thickness is 670. The computed results show good agreement with direct numerical simulation (DNS), which include root mean square fluctuated velocity distribution and average velocity distribution. It is also found that the staggered phenomenon of the coherent structures is caused by sub-harmonic. The results clearly show the formation and evolution of horseshoe vortex in the turbulent boundary layer, including horseshoe vortex structure with a pair of streamwise vortexes and one-side leg of horseshoe vortex. Based on the results, the development of the horseshoe-shaped coherent structures is analyzed in turbulent boundary layer.

Key words: large eddy simulation (LES); horseshoe-shaped vortex; turbulent boundary layer; coherent structures; preconditioned algorithm

CLC number: O354.9; V211.3 **Document code**: A **Article ID**: 1005-1120(2011)01-0048-09

INTRODUCTION

Near-wall region in the turbulent boundary layer, coherent structure is the most active large-scale movement in this area. Many of the fluid macro-features, such as the generation and maintenance of turbulence, the transport and dissipation of turbulence energy, the resistance decreases, heat transfer and so on, are closely related with coherent structures in the wall boundary layer[1]. Numerical experimental and simulation results show that the streamwise vortex structure is the typical feature of the coherent structure in turbulent boundary layer[2]. In numerous streamwise vortex structures, the horseshoe-shaped vortex (or hairpin vortex), in particular, received widespread attention[3-4]. Therefore, studying evolution of the horseshoe-shaped vortex can provide a lot of reasonable explanation for flow phenomena within the turbulent boundary layer, and help to in-depth understand and resolve problems encountered in the engineering flow.

In the past, people thought that such the horseshoe-shaped vortex (or hairpin vortex) could be represented by using a pair of symmetric counter-rotating vortexes[5]. However, recent studies have found[1,6-7] that not only symmetric vortex pairs, but also asymmetric vortex pairs exist in the coherent structure in turbulence flow zone near the wall, and the asymmetric vortex pair is the vast majority of the streamwise vortex pairs. Note that the horseshoe and the hairpin can be connected by a function of Reynolds number, and the low-Reynolds-number structure is referred to as the horseshoe-shaped vortex[6,8]. At present, large eddy simulation (LES) can display

Foundation item: Supported by the National Natural Science Foundation of China (10772082).

Received date: 2010-10-18; **revision received date**: 2011-01-02

E-mail: shi12345love@163.com

the details of flow field and transient process, and the required CPU hours are less than the direct numerical simulation, so the LES method is used in this paper.

For the LES turbulence simulations, if the computation is started from the laminar flow through the transition to turbulent flow, calculation turbulent fluid need to attach a great amount of computational resources. Therefore, a given 3-D disturbance wave method[9-10] is used for LES of turbulent inlet boundary to simulate 3-D turbulent flow in channel. The result of LES is compared with the direct numerical simulation (DNS) results to verify the effective of the LES method. On this basis, the horseshoe-shaped vortex structures in the near-wall turbulence are studied.

1 NUMERICAL METHODS

1.1 Governing equations and discretization

The code is used LES with a preconditioned algorithm[11]. After Faver-average and filter, the Navier-Stokes equation is transformed to a curvilinear system of coordinates. The non-dimensional vector forms of 3-D large eddy simulation of compressible flow equations are

$$M\,\Gamma^{-1}\boldsymbol{J}\,\frac{\partial \boldsymbol{q}}{\partial \tau}+\boldsymbol{J}\,\frac{\partial \boldsymbol{Q}}{\partial t}+\frac{\partial \boldsymbol{F}_j}{\partial \kappa_j}=0 \tag{1}$$

$$\boldsymbol{F}_j=\boldsymbol{J}\begin{bmatrix}\overline{\rho}\,\widetilde{U}_j\\ \overline{\rho}\,\tilde{u}_1\,\widetilde{U}_j+\overline{p}\,\kappa_{x1}^j+\kappa_{xi}^j(\tau_{1i}-\dfrac{1}{Re}\,\tilde{\sigma}_{1i})\\ \overline{\rho}\,\tilde{u}_2\,\widetilde{U}_j+\overline{p}\,\kappa_{x2}^j+\kappa_{xi}^j(\tau_{2i}-\dfrac{1}{Re}\,\tilde{\sigma}_{2i})\\ \overline{\rho}\,\tilde{u}_3\,\widetilde{U}_j+\overline{p}\,\kappa_{x3}^j+\kappa_{xi}^j(\tau_{3i}-\dfrac{1}{Re}\,\tilde{\sigma}_{2i})\\ \widetilde{U}_j[\overline{\rho}\,\tilde{e}+(\gamma-1)Mr^2\,\overline{p}]-(\gamma-1)\cdot\\ Mr^2\,\widetilde{T}_{\kappa_{ji}}\,\tilde{u}_i+\kappa_{xi}^j(\dfrac{1}{Re}q_i+q_i^{\mathrm{SGS}})\end{bmatrix}$$
$$i,j=1,2,3 \tag{2}$$

where $M=\partial\boldsymbol{Q}/\partial\boldsymbol{q}$, $\boldsymbol{q}=[\overline{\rho},\tilde{u}_1,\tilde{u}_2,\tilde{u}_3,\overline{p}]^{\mathrm{T}}$ is the primitive variable, $\boldsymbol{Q}=[\overline{\rho},\overline{\rho}\,\tilde{u},\overline{\rho}\,\tilde{v},\overline{\rho}\tilde{w},\overline{\rho}\,\tilde{e}\,]^{\mathrm{T}}$ the conservation variables, and $\Gamma=\mathrm{diag}\{1\ 1\ 1\ 1\ \beta(Mr)\}$ the preconditioning matrix. The preconditioning parameter β, if $Mr<1.0$, $\beta(Mr)=Mr^2$; if $Mr\geqslant 1.0$, $\beta(Mr)=1.0$. $Mr^2=\hat{u}^2/(\gamma R\hat{T})$ is characterized Mach number, $Re=\hat{\rho}\,\hat{u}\,\hat{L}/\hat{\mu}$ the characterized Reynolds number, $\kappa_{x_i}^j=\partial\kappa_j/\partial x_i$, $\tau_{ij}=\overline{\rho}(\widetilde{u_iu_j}-\tilde{u}_i\,\tilde{u}_j)$ the subgrid viscous stress, and q_i^{SGS} the subgrid heat flux. Jacobian matrix transformation matrix is $\boldsymbol{J}=\det\left|\dfrac{\partial(x,y,z)}{\partial(\xi,\eta,\zeta)}\right|$.

In this paper, the preconditioned algorithm is used, which can improve low Mach number calculated method of the near-wall flow on the stability and convergence behavior. The governing equations are discreted by the used finite volume method. Viscous fluxes adopts the second-order center scheme. Inviscid fluxes adopts the six-order accurate symmetric WENO scheme. The third-order Runge-Kutta method is used for the time scheme.

1.2 Dynamic subgrid-scale model

The key of LES is to establish a rational subgrid model. The most widely used subgrid-scale model is the Smagorinsky eddy-viscosity model[12]

$$\tau_{ij}=\overline{\rho}(\widetilde{u_iu_j}-\tilde{u}_i\,\tilde{u}_j)=-2C\,\overline{\rho}\Delta^2|\tilde{S}|\,\tilde{S}_{ij}+\frac{1}{3}\delta_{ij}\tau_{kk} \tag{3}$$

where $\tilde{S}_{ij}=\dfrac{1}{2}\left(\dfrac{\partial\tilde{u}_i}{\partial x_j}+\dfrac{\partial\tilde{u}_j}{\partial x_i}\right)$, $|\tilde{S}|=\sqrt{2\,\tilde{S}_{ij}\,\tilde{S}_{ij}}$ is the magnitude of large-scale strain-rate tensor, $\tilde{u}_i$ the large-scale velocity, and Δ the filter width. Generally, C is taken as a constant 0.01. In low-mach flow, the last item of the right side included in the pressure item does not require simulation, so subgrid viscosity can be expressed as

$$\mu^{\mathrm{SGS}}=C\overline{\rho}\Delta^2|\widetilde{S}| \tag{4}$$

The corresponding subgrid heat flux is as follows

$$q_k^{\mathrm{SGS}}=-\frac{\mu^{\mathrm{SGS}}}{Pr_t}\frac{\partial T}{\partial x_k} \tag{5}$$

But the Smagorinsky model has obvious shortcomings, such as the coefficient of C is case related rather than the constant optimum C value depending on the actual nature of fluid movement, and the compressible flow model does not reflect fluid compressibility. Therefore, the dynamic subgrid model proposed by Germano is

used in this paper, and the specific equations are as follow[12].

The key of dynamic model is to determine a dynamic subgrid eddy viscosity coefficient C. There is a hypothesis that the stress of the smallest pulse on the coarse grid is equal to the subgrid stress difference between the coarse grid and the fine grid. On the basis, by using twice filtering to Navier-Stokes equations and the least square method, we obtain

$$C = \left\langle \frac{M_{ij}L_{ij}}{M_{ij}M_{ij}} \right\rangle \tag{6}$$

where

$$\begin{cases} L_{ij} = (\widehat{\widetilde{\rho u_i}\,\widetilde{\rho u_j}/\overline{\rho}} - \widehat{\widetilde{\rho u_i}}\,\widehat{\widetilde{\rho u_j}}/\hat{\overline{\rho}}) - \\ \qquad \frac{1}{3}\delta_{ij}(\widehat{\widetilde{\rho u_i}\,\widetilde{\rho u_j}/\overline{\rho}} - \widehat{\widetilde{\rho u_i}}\,\widehat{\widetilde{\rho u_j}}/\hat{\overline{\rho}}) \\ M_{ij} = -2(\hat{\overline{\rho}}\,\hat{\Delta}^2|\hat{\overline{S}}|\hat{\overline{S}}_{ij} - \widehat{\overline{\rho}\Delta^2|\overline{S}|\overline{S}_{ij}}) \end{cases}$$

The superscript "^" denotes the filtering of coarse grid, "~" the filtering of fine grid. The sign "< >" indicates that the average of both sides are taken over a plane parallel to the wall.

2 COMPUTATIONAL DOMAIN AND BOUNDARY CONDITIONS

The boundary layer of the compressible turbulent channel flow is calculated by dimensionless curvilinear coordinate LES equations. Mach number is set to 0.6. Reynolds number at the inflow is 1 000 based on the displacement thickness δ^* and the free-stream velocity, that is, Reynolds number is 670 based on the momentum thickness θ.

2.1 Computational domain

Computational domain is shown in Fig. 1. The displacement thickness δ^* of turbulent boundary layer of inlet is selected as a characteristic length. A uniform grid of $192\times96\times64$ is used to model the computational domain with the dimensionless size of $50\times10\times8$, respectively, corresponding to the streamwise direction X, the normal direction Y and the spanwise direction Z. The grid is uniformly distributed in the streamwise and spanwise directions and stretched in the wall-normal direction. In order to facilitate parallel computing, grid is divided into four parts and each part is calculated on CPU which number sequence is from zero to three (Fig. 1). MPI is used to deliver the exchange of information between the parts.

Flow field is initialized in the Spalding's turbulent boundary layer mean velocity profile. At the subsonic outflow, a fixed back pressure is prescribed. Periodic boundary conditions are used in the spanwise direction. At the upper surface, a free-slip boundary condition is applied. At the lower wall, a no-slip condition is used for the velocity components and an adiabatic wall condition is prescribed. Therefore, only the half-height channel domain is given in the direction Y in Fig. 1.

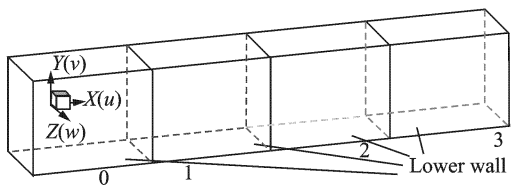

Fig. 1 Schematic of parallel computational domain decomposition

2.2 Inlet boundary condition

A given 3-D disturbance wave method in inlet of the calculation domain is used. This approach is based on the assumption that the turbulence is a combination of coherent structures, which is recognized by the researchers. It produces a set of disturbance waves, including changes in time and space coherent structures in the inlet. This method is simpler than the other current turbulence inlet method and more suitable in the engineering-oriented.

For the inlet boundary conditions, the key is to determine the entrance instantaneous velocity. The inflow instantaneous velocity is given in the form of: instantaneous value equals average value plusing disturbance and random noise. For the average value, the 2-D Spalding-like turbulent velocity profile is used. The maximum amplitude of random noise does not exceed the average free-flow speed of 1%.

A given directly 3-D wave can determine the disturbance $\hat{u}(x,y,z,t)$. The method reproduces the dynamical features of the inner and outer part of the boundary-layer, including lifted "streaks" and coherent outer-layer motions. The outer-layer is expressed a 3-D disturbance wave[7,9] which is a combination of fundamental wave and subharmonics. Its formula[9] and the selection of parameters are

$$\hat{u}^{\text{inner}} = c_{1,0}y^{+}\,\mathrm{e}^{-y^{+}/y^{+}_{p,0}}\sin(\omega_0 t)\cos(\beta_0 z+\phi_0) \quad (7)$$

$$\hat{v}^{\text{inner}} = c_{2,0}(y^{+})^{2}\mathrm{e}^{-(y^{+}/y^{+}_{p,0})^{2}}\sin(\omega_0 t)\cos(\beta_0 z+\phi_0) \quad (8)$$

$$\hat{u}^{\text{outer}} = \sum_{j=1}^{3} c_{1,j}y/y_{p,j}\mathrm{e}^{-y/y_{p,j}}\sin(\omega_j t)\cos(\beta_j z+\phi_j) \quad (9)$$

$$\hat{v}^{\text{outer}} = \sum_{j=1}^{3} c_{1,j}(y/y_{p,j})^{2}\mathrm{e}^{-(y/y_{p,j})^{2}}\sin(\omega_j t)\cdot \cos(\beta_j z+\phi_j) \quad (10)$$

where the spanwise velocity w is derived from a divergence-free condition. ω_j stands for forcing characteristic frequency, β_j the spanwise wave numbers, and ϕ_j the phase shifts. Table 1 gives a summary of the parameters used in the boundary-layer simulation.

Table 1 Parameters for inflow turbulent fluctuations for turbulent boundary layer

Region	j	c_{1j}	c_{2j}	ω_j	β_j	ϕ_j	$y^{+}_{p,j}$	$y_{p,j}$
Inner	0	0.1	−0.001 6	1/25	π	0.00	12	—
Outer	1	0.2	−0.120 0	1/4	0.75π	0.00	—	1
	2	0.2	−0.120 0	1/8	0.50π	0.10	—	4
	3	0.2	−0.120 0	1/16	0.25π	0.15	—	8

3 RESULT ANALYSIS AND DISCUSSION

Turbulent boundary layer structure is 3-D. The outer edge has a shortcoming of free shear layer. There is an interaction between the inner and outer. The inner layer is inhibited by the wall. So the flowing structure within the turbulent boundary layer is very complex. The calculated results are compared with the DNS results to verify the effective of the result. Then the turbulent boundary layer horseshoe-shaped vortex coherent structures are analyzed. In this paper, Mach number is set to 0.6. Reynolds number is 670 based on the momentum thickness θ, that is, Reynolds number at the inflow is 1 000 based on the displacement thickness δ^{*} and the free-stream velocity.

3.1 Time-average velocity and surface friction coefficient

Time- and spanwise-averaged streamwise velocity profiles are shown in Fig. 2(a). The result accords with the same Reynolds number of the

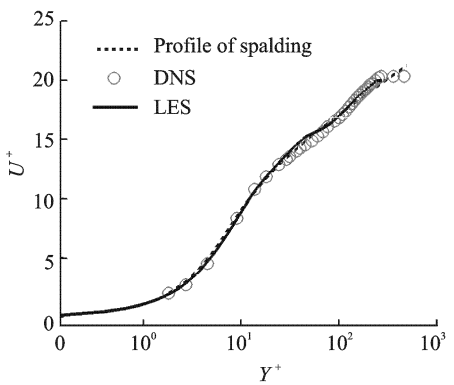

(a) Time- and spanwise-averaged streamwise velocity profile

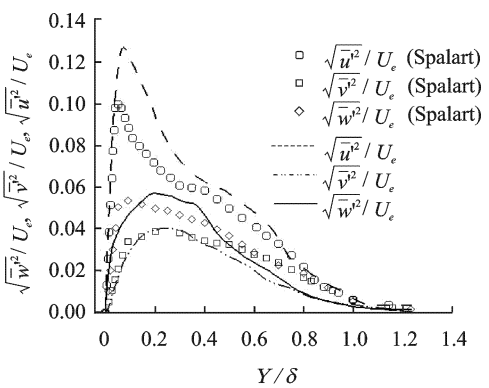

(b) Root mean square of fluctuations velocity

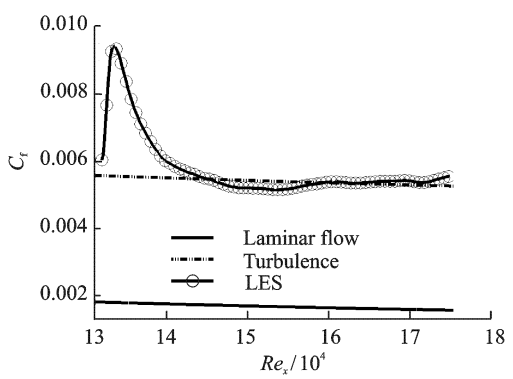

(c) Skin-friction coefficient

Fig. 2 Turbulent boundary-layer simulation results

DNS solution[13] very well. The comparison indicates that the inlet section develops a stable turbulence after the short development.

Time- and spanwise-averaged turbulent fluctuation velocity is displayed in Fig. 2(b). The superscript "′" indicates the fluctuation value. U_e is the streamwise velocity outside the boundary layer. The LES result is compared with Spalart's DNS turbulence solution[13]. It is found that the results are in good agreement with the DNS solution in all directions, but the amplitude of the streamwise fluctuation velocity has some deviations. This reason may that the DNS solution is incompressible flow calculation results, while the LES result is the compressible one.

Fig. 2(c) shows the time-average and spanwise-average surface-friction coefficient C_f. It can be seen after only a short interim from the entrance. When Re_x reaches 139 000, C_f shows a good agreement between numerical and experimental results of turbulence. The fluctuation of C_f during and after the transition represents the unsteadiness of turbulent flow.

3.2 Discussion of turbulent boundary layer horseshoe-shaped coherent structure

The horseshoe-shaped coherent structures within the boundary layer are analyzed in this section. The time showed in the figures in this section is the dimensionless value based on a time units. Since the vortex cores are associated with strong vorticity and local pressure minima, it can be readily shown that positive surfaces of the Laplacian of pressure[14] can be used to identify coherent structures.

3.2.1 Oscillating streamwise vortex of process of vortex formation of horseshoe-shaped vortex

In the paper, there are many vortex structures and these streamwise vortex structures are closely related with low-speed zones. Fig. 3 shows that at the dimensionless time $t=6.62T$, vortex structures are compared with velocity contours in the flow field. It is clear to see that the streamwise vortex structure corresponds with low-velocity zones. The streamwise vortex in the x-z plane is swing, and therefore low-speed streaks are swing and not beeline. This is the same conclusion as that in Refs. [7,15].

Fig. 4 shows the generation of the horseshoe-shaped structures by a pair of streamwise vortex. As mentioned in Fig. 3, the streamwise vortex structures swing along the streamwise. In Fig. 4, when the two streamwise vortexes (the two-leg vortexes) close to each other, the head of two vortex will generate a bridge between the two leg, and then the two vortexes change into the horseshoe-shaped vortex structure. There is the same solution in Ref. [4].

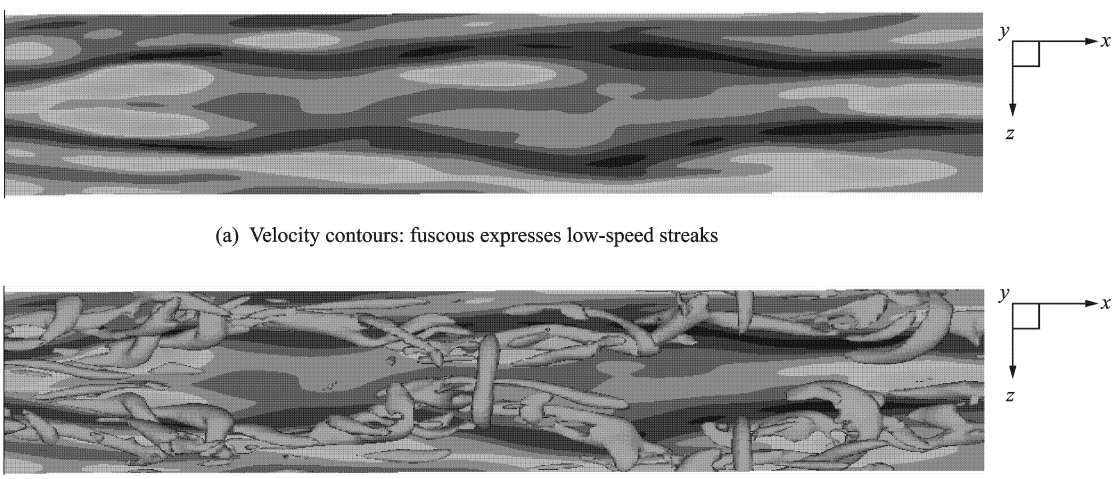

(a) Velocity contours: fuscous expresses low-speed streaks

(b) Coherent structures

Fig. 3 Top view of coherent structures and low-speed streaks in flow field ($t=6.62$)

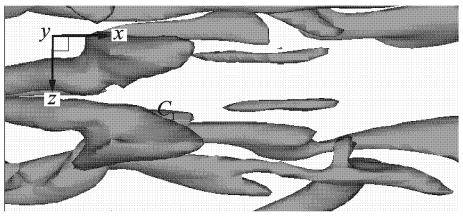

(a) $t = 5.90$

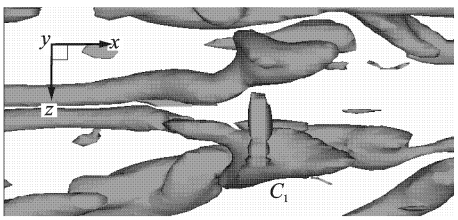

(b) $t = 5.91$

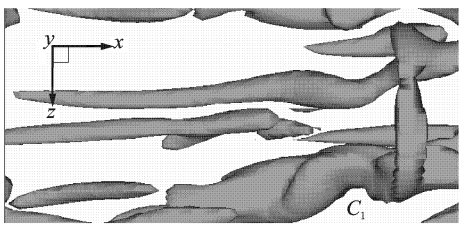

(c) $t = 5.92$

Fig. 4 Generation of horseshoe-shaped structures by pair of streamwise vortex

Two streamwise vortex legs close to each other will form a larger horseshoe vortex structure. However, if two vortex legs distance is so longer, the head of horseshoe vortex structure will not be closed, and there is the middle of opening. Eventually, the horseshoe-shaped vortex is generated by the one-side streamwise vortex. The process is shown in Fig. 5 that F_1 and F_2 structures are developed from a tilted vortex along streamwise to a horseshoe-shaped vortex. In Fig. 5(a), F_1 is a streamwise vortex. The vortex head of the streamwise vortex under the action of the self-induced upward rises, at the same time the head tilts to one side of the vortex. Fig. 5(b) shows that the vortex head that slants toward spanwise is elongated along spanwise. So the vortex tube of the part of vortex head is thinner and draws out along spanwise. In Fig. 5(c, d), when the spanwise head of the vortex is stretching, the head comes into being a horseshoe vortex owing to the effect of the disturbance. Fig. 5(d-f) show the forming process that the

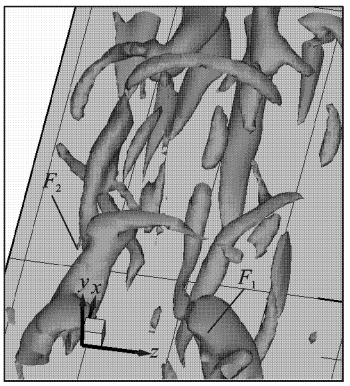

(a) $t = 5.91$

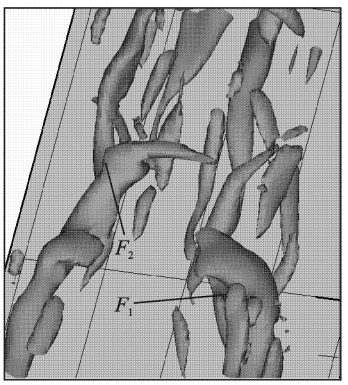

(b) $t = 5.92$

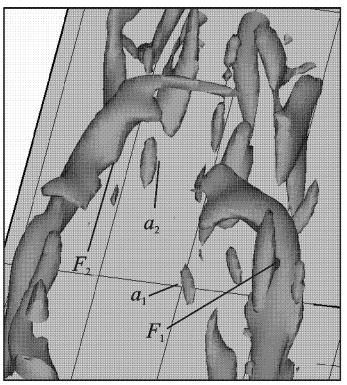

(c) $t = 5.93$

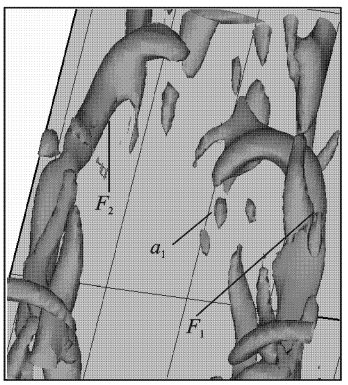

(d) $t = 5.94$

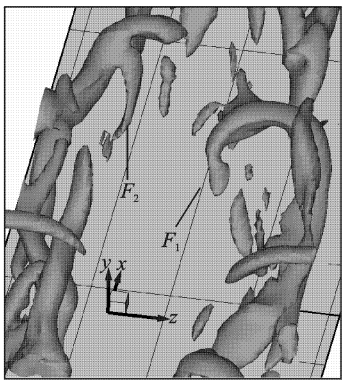

(e) $t = 5.95$

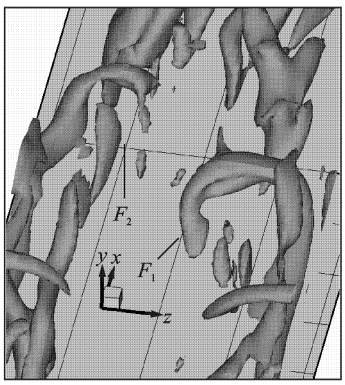

(f) $t = 5.96$

Fig. 5 Generation of horseshoe-shaped vortex by one-side streamwise vortex

shorter leg of one-side horseshoe-shaped vortex evolved. Robinson (1991) described the similar process[16] that the neck of horseshoe vortex moved to the wall and the descending neck was rapidly stretched into an elongated vortex leg. In Figs. 5(c-f), when the neck is moving, down and stretching, a slender vortex tube (a_1) occurs on the shorter leg side of the horseshoe vortex and is an extended vortex leg. The vorticity of the leg is very weak, so the leg seems broken. In the paper, the inflow boundary conditions are generated by the flow of counter-rotating vortex pair, so the one-side generated horseshoe vortex structures are always in pairs.

Fig. 6 shows the velocity field of the leg of the horseshoe-shaped coherent structures. Two streamwise-vortex legs of F_1 horseshoe vortex is counter-rotating. So the upward ejection occurs between two streamwise-vortex legs, and the downward sweep occurs on the two vortex legs

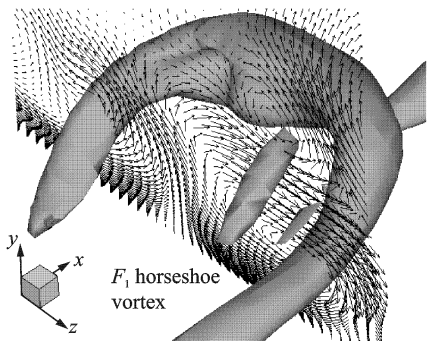

Fig. 6 Velocity field of leg of horseshoe-shaped coherent structure

lateral. While some broken streamwise vortex also exist between two vortex legs. The fluid has a similar formation in upward ejection and downward sweep.

3.2.2 Horseshoe-shaped vortex structure under influence of sub-harmonic

Fig. 7 shows that the coherent structures exist in the turbulent flow. The calculation results are expanded along one spanwise width in order to better observe the spanwise coherent structures on the boundary. The first 1/4 part of the entire computational domain is short development section (Fig. 7(a)). The showed horseshoe vortexes are after the development segment. There are many horseshoe-shaped vortexes within the turbulent flow field. But the horseshoe-shaped shape of the structure is not uniform and is not strict symmetry. The reason is mainly the unsteady

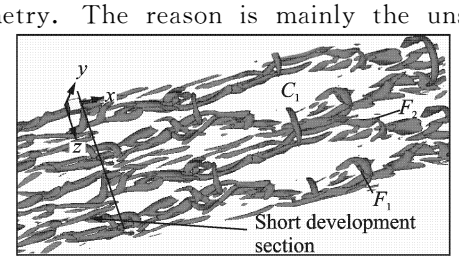

(a) $t = 6.72$

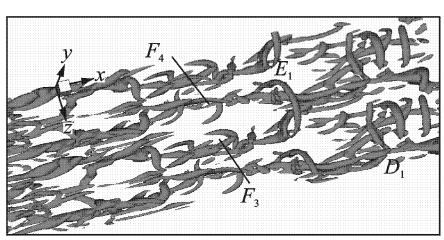

(b) $t = 7.12$

Fig. 7 Unsteady dynamics of coherent structures at different time instants

characteristic of turbulence. This conclusion is the same as that in Refs. [1,5].

Fig. 7 shows two different time points of coherent structures. The English capital letter sequences denote the pair-vortex generated horseshoe-shaped vortex structure under the influence of the sub-harmonics. As shown in Fig. 7, it is found that there are several complex horseshoe-shaped vortexes (such as the identified coherent structures from C_1 to E_1, the development of C_1 is shown in Fig. 4.) in near-wall region. However the basic features of the flow expresse a staggered pattern caused by sub-harmonic instability, i.e., and the spanwise disposition of the former structure and latter structure is staggered distribution along the direction x. In addition, it is also found that there are the one-side generated horseshoe-shaped vortex structures between two pair-vortex generated horseshoe-shaped vortex structures in Fig. 7 (such as the identified coherent structures from F_1 to F_4, the development of F_1 is shown in Fig. 5). At the same time, the non-uniform long streamwise vortex structures appear between the two group configuration rows, and the vortex structure is always swing, rather than simply move forward along the streamwise.

4 CONCLUSIONS

In this paper, turbulent channel flow is calculated using LES with the preconditioned algorithm and the dynamic subgrid-scale model. The spatial discretization scheme used high-order symmetric WENO scheme of finite volume method. The time-discrete used the third-order Runge-Kutta method. A given perturbation method is used inlet.

(1) The LES calculation results are compared with the DNS solution, which include the average speed profile, turbulence intensity distribution and skin-friction coefficient. The above comparison verify the validity of the LES results.

(2) The streamwise vortex structures correspond with the low velocity zones. The streamwise vortex in the x-z plane is oscillatory and side-to-side meandering. Therefore swing low-speed streaks are not about pure streamwise direction. In addition, the streamwise vortexes are not only individual evolution but also the interactions in the development process along the downstream. The individual evolution is the generation of the horseshoe-shaped vortex by the one-side streamwise vortex and the interactions is the generation of the horseshoe-shaped vortex by a pair of streamwise vortex.

(3) The LES calculation results demonstrate the horseshoe-shaped vortex configurations. The pair-vortex generated horseshoe-shaped vortex structure under the influence of the sub-harmonics is expressed a staggered pattern. The horseshoe-shaped vortex structure is not strict symmetry.

(4) Downward sweep and upward ejection are induced by the up-tilt streamwise-vortex legs.

References:

[1] Lu Changgeng. Comparison of symmetrical and unsymmetrical single coherent structure evolution mechanism in wall region of turbulence boundary layer[J]. Journal of Hydrodynamics, 2005, A20(4): 442-445. (in Chinese)

[2] Zhang Nan, Lu Lipeng, Duan Zhenzhen, et al. Numerical simulation of Quasi-streamwise Hairpin-like vortex generation in a turbulent boundary layer[J]. Applied Mathematics and Mechanics, 2008, 29(1): 13-20. (in Chinese)

[3] Zhou J, Adrian R J, Balachandar S, et al. Mechanisms for generating coherent packets of hairpinvortices in channel flow[J]. J Fluid Mech, 1999, 387: 353-396.

[4] Chen Lin, Tang Dengbin, Liu Xiaobing, et al. Evolution of the ring-like vortices and spike structure in transitional boundary layers[J]. Sci China (Ser G), 2009, 39(10): 1520-1526.

[5] Cantwell B J. Organized motions in turbulent flows [J]. Annual Review of Fluid Mechanics, 1981, 13: 457-515.

[6] Greeen S I. Fluid vortices[M]. Dordrecht: Kluwer Academic Publishers, 1995.

[7] Zhou Heng, Xiong Zhongmin. The mechanism for the generation of coherent strutures in the wall region of a turbulent boundary layer[J]. Science in China (Series A), 1994, 24(9): 941-948.

[8] Delo C J, Kelso R M, Smits A J. Three-dimensional structure of a low-Reynolds-number turbulent boundary layer[J]. J Fluid Mech, 2004, 512:47-83.

[9] Sandham N D, Yao Y F, Lawal A A. Large-eddy simulation of transonic turbulent flow over a bump [J]. Inernational Journal of Heat and Fluid Flow, 2003, 24:584-595.

[10] Zhou Heng. Instability waves in the wall region of a turbulent boundary layer on a flat plate[J]. Chinese Journal of Theoretical and Applied Mechanics, 1988, 20(6):481-488. (in Chinese)

[11] Briley W R, Taylor L K, Whitfield D L. High-resolution viscous flow simulations at arbitrary Mach mumber [J]. Journal of Computational Physics, 2003, 184(1):79-105.

[12] Germano M, Piomelli U, Moin P, et al. A dynamic subgrid-scale eddy viscosity model[J]. Physics of Fluids, 1991, 3: 1760-1765.

[13] Spalart P R. Direct simulation of a turbulent boundary layer up to $Re_\theta=1410$[J]. Journal of Fluid Mechanics, 1988, 187:61-98.

[14] Tyagi M, Acharya S. Large eddy simulation of film cooling flow from an inclined cylindrical jet [J]. ASME, 2003,125: 734-742.

[15] Schoppa W, Hussain F. Numerical study of near-wall coherent structures and their control in turbulent boundary layers [C]//Sixteenth International Conference on Numerical Methods in Fluid Dynamics. [S. l.]:Springer-Verlag, 1998:103-116.

[16] Robinson S K. Coherent motions in the turbulent boundary layer[J]. Ann Rev Fluid Mech, 1991,23: 601-639.

湍流边界层近壁区马蹄涡拟序结构的数值模拟与分析

史万里[1] 葛 宁[1] 陈 林[2] 唐登斌[2]

(1. 南京航空航天大学能源与动力学院,南京,210016,中国;
2. 南京航空航天大学航空宇航学院,南京,210016,中国)

摘要:采用大涡模拟对低雷诺数槽道湍流进行了数值模拟,进口边界条件采用了给定扰动波方法,经过短过渡段得到完全发展湍流。计算中采用了动态亚格子模型和预处理技术,进口采用的动量厚度雷诺数是670。大涡模拟对计算得到的平均速度剖面以及脉动分量与DNS解进行对比,验证了计算结果的可靠性。计算结果显示了湍流场中马蹄涡的形成及演化过程,其中包括形成单腿马蹄涡和形成对称涡腿的马蹄涡,同时发现流场中存在由亚谐波引起的拟序结构的交错现象,并在此基础上分析了湍流边界层近壁区马蹄涡结构的演化。

关键词:大涡模拟; 马蹄涡; 湍流边界层; 拟序结构; 预处理算法

中图分类号:O354.9; V211.3

(Executive editor: Sun Jing)

基金项目:国家自然科学基金(10772082)资助项目。